Precision measurements using squeezed spin states via two-axis countertwisting interactions

Emi Yukawa,[1] G. J. Milburn,[2] C. A. Holmes,[3] Masahito Ueda,[4] and Kae Nemoto[1]
[1]*National Institute of Informatics, 2-1-2 Hitotsubashi, Chiyoda-ku, Tokyo 101-8430, Japan*
[2]*Centre for Engineered Quantum Systems, School of Mathematics and Physics, The University of Queensland, St. Lucia, Queensland 4072, Australia*
[3]*School of Mathematics and Physics, University of Queensland, Queensland 4072, Australia*
[4]*Department of Physics, University of Tokyo, 7-3-1 Hongo, Bunkyo-ku, Tokyo 113-0033, Japan*
(Received 24 October 2014; published 29 December 2014)

We show that the two-axis countertwisting interaction squeezes a coherent spin state into three states of interest in quantum information, namely, the equally weighted superposition state, the state close to the twin-Fock state, and the state achieving the Heisenberg limit of optimal sensitivity defined by the Cramér-Rao inequality, in addition to the well-known Heisenberg-limited state of spin fluctuations.

DOI: 10.1103/PhysRevA.90.062132 PACS number(s): 03.65.Ta, 42.50.Lc, 07.55.Ge

I. INTRODUCTION

Squeezed states have been intensively investigated originally in optics and extended to various bosonic and spin systems. A defining feature of squeezing is to enhance the quantum nature, such as reduced quantum noise and entanglement, which forms the basis of their applications, for instance, high-precision measurements [1,2]. While entanglement is not always the key in high-precision measurements [3], some of these implementations are expected to surpass the standard quantum limit.

There are other quantum states proposed for high-precision measurements, such as a superposition state of coherent states [4], squeezed spin states (SSSs) [5], and other spin ensemble states [6–14]. These states may also achieve sensitivity beyond the standard quantum limit. Among them, the advantage of spin squeezing is its feasible implementation of the state [15–25]. For instance, spin squeezing by one-axis twisting has been experimentally realized in cold-atomic systems [16–22,24] and has been proposed in nitrogen-vacancy-spin ensembles [25]. Furthermore, spin fluctuations below the standard quantum limit have been observed [20,21]. Meanwhile, spin squeezing by the two-axis countertwisting method [5] has not been realized; however, there are some experimental proposals in realistic systems [9,26–32].

The minimum quantum fluctuations of the SSSs have been thoroughly investigated; however, the sensitivity of measurements utilizing the SSSs, which should also be discussed in terms of estimation theory [33–35], has not been fully analyzed. The precision of a measurement can be estimated by the standard deviation of a measurement-and-estimation process, which satisfies the Cramér-Rao inequality [36,37]. Similarly to the Heisenberg limit for quantum spin fluctuations, we can define the Heisenberg limit of the minimum standard deviation using the Cramér-Rao inequality. For the total spin size of J of spin-1/2 particles, a coherent spin state (CSS) gives the minimum standard deviation which is proportional to $J^{-1/2}$, and one-axis twisting brings the state to the Heisenberg limit with the variance given by J^{-1} [33].

In this article, we investigate the time evolution of SSSs in a spin-1/2 ensemble through the two-axis countertwisting interaction [5] and the optimal sensitivity in high-precision measurements. Similarly to the one-axis twisting case [33], we expect that the SSS will change the sensitivity though time evolution. We will numerically show that, depending on the evolution time of the two-axis countertwisting interaction, we can generate an SSS that has high fidelity to the equally weighted superposition state (EWSS) [10] or an SSS close to the twin-Fock state [6,13]. Both states can be used for high-precision measurements with Heisenberg-limited sensitivity and are not easily implemented experimentally. We will also numerically obtain the sensitivities for these SSSs and the SSS optimizing the sensitivity with respect to the evolution time, and compare them with the EWSS, the twin-Fock state, and the cat state.

This paper is organized as follows. In Sec. II, we briefly explain the two-axis countertwisting interactions. In Sec. III, we numerically show that the two-axis countertwisting interaction brings a CSS to a state with high fidelity to the EWSS or the twin-Fock state. In Sec. IV, we numerically obtain a time evolution of optimal precision using SSSs and discuss the scaling of the precision with respect to J. In Sec. V, we summarize the main results of this article. The effect of a dc magnetic field on two-axis countertwisting is discussed in the Appendix to avoid digressing from the main subjects.

II. TIME EVOLUTION OF A COHERENT SPIN STATE UNDER A TWO-AXIS COUNTERTWISTING INTERACTION

We consider an SSS generated from a CSS via a two-axis countertwisting interaction. Here, we assume an ensemble of N spin-1/2 particles as a system. With two real parameters α and β, a CSS is given by $|\Psi_{\rm CSS}(\alpha,\beta)\rangle = \bigotimes_{i=0}^{N} |\psi(\alpha,\beta)\rangle_i$, where $|\psi(\alpha,\beta)\rangle_i = \cos\frac{\beta}{2}|\uparrow\rangle_i + e^{i\alpha}\sin\frac{\beta}{2}|\downarrow\rangle_i$. The suffix i denotes the ith 1/2 spin and $|\uparrow\rangle_i$ and $|\downarrow\rangle_i$ are the eigenstates of the Pauli matrix $\hat{\sigma}_z^{(i)}$ for the eigenvalues of ± 1, respectively. We introduce the collective spin operator $\hat{\boldsymbol{J}} \equiv \sum_{i=0}^{N} \frac{1}{2}\hat{\boldsymbol{\sigma}}^{(i)}$ and expand the CSS in terms of the eigenstates of $\hat{J}_z$, yielding

$$|\Psi_{\rm CSS}(\alpha,\beta)\rangle = \sum_{M=-J}^{J} \sqrt{{}_{2J}C_{J-M}}\, e^{i(J-M)\alpha} \cos^{J+M}\frac{\beta}{2} \sin^{J-M}\frac{\beta}{2} |J,M\rangle, \quad (1)$$

where $J = N/2$ and $|J,M\rangle$ represents the eigenstate of $\hat{J}_z$ with the eigenvalue of M. We set α and β to be zero such that the

initial CSS is fixed to $|J,J\rangle$. Then, the two-axis countertwisting Hamiltonian can be expressed in terms of the collective spin operators as

$$\hat{H}_{\rm TAT} = \frac{\hbar\chi}{2i}(e^{-2i\gamma}\hat{J}_+^2 - e^{2i\gamma}\hat{J}_-^2), \tag{2}$$

where χ is the strength of the interaction, $\hat{J}_\pm$ denotes the spin-J ladder operators, and γ determines the orientation of spin squeezing. For the sake of simplicity, we choose $\chi = 1$ and $\gamma = 0$, setting the squeezing axis to be J_y. We begin with the initial coherent state $|J,J\rangle$, let it evolve for a certain time τ, and then rotate it along the y axis by $\pi/2$; hence the resulting state is

$$|\Psi_{\rm SSS}(\tau)\rangle_x = e^{-i\frac{\pi}{2}\hat{J}_y}e^{-\frac{i}{\hbar}\hat{H}_{\rm TAT}\tau}|J,J\rangle. \tag{3}$$

III. COMPARISON WITH THE EQUALLY WEIGHTED SUPERPOSITION STATE AND THE TWIN-FOCK STATE

First, we evaluate the SSS in Eq. (3) at a certain evolution time τ, when the SSS has the first local maximum of fidelity to the EWSS [10] or the twin-Fock state [6,13], as shown in Fig. 1. Here, the fidelity of the SSS in Eq. (3) to the state $|\Psi_X\rangle$ is given by $F_X(\tau) = |\langle\Psi_X|\Psi_{\rm SSS}(\tau)\rangle_x|^2$ as a function of the evolution time τ in Eq. (3). The EWSS and the twin-Fock state (TFS) are given by

$$|\Psi_{\rm EWSS}\rangle \equiv \frac{1}{\sqrt{2J+1}}\sum_{M=-J}^{J}|J,M\rangle \tag{4}$$

and

$$|\Psi_{\rm TFS}\rangle \equiv e^{-i\frac{\pi}{2}\hat{J}_x}|J,0\rangle, \tag{5}$$

respectively. The fidelity functions $F_{\rm EWSS}(\tau)$ and $F_{\rm TFS}(\tau)$ are maximized at certain evolution times $\tau_{\rm EWSS}$ and $\tau_{\rm TFS}$ for a fixed collective spin J. We refer to the SSSs at evolution times $\tau_{\rm EWSS}$

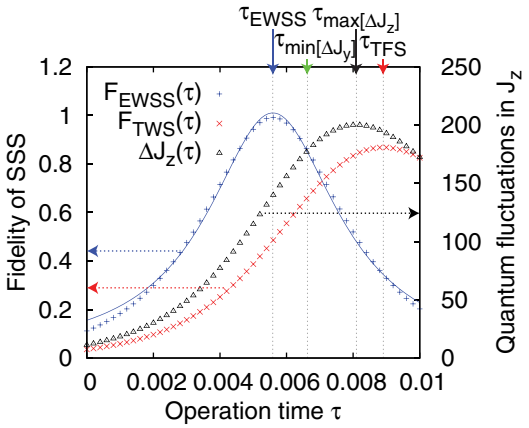

FIG. 1. (Color online) Plots of the fidelity to the EWSS $F_{\rm EWSS}(\tau)$, the fidelity to the twin-Fock state $F_{\rm TFS}(\tau)$, and the quantum fluctuations $\langle(\Delta J_z)^2\rangle_{\rm SSS}^{1/2}(\tau)$ for $J = 250$ as functions of the evolution time τ around their first local maxima. The fidelity to the EWSS $F_{\rm EWSS}(\tau)$ around the maximum can be well fitted to the Lorentzian function with a full width at half maxima (FWHM) of $\sim 2/(3J)$, which is indicated by the blue solid curve.

and $\tau_{\rm TFS}$ as those optimized to the EWSS and the twin-Fock state, respectively. We numerically obtain $F_{\rm EWSS}(\tau_{\rm EWSS})$ and $F_{\rm TFS}(\tau_{\rm TFS})$ and plot them in Fig. 2(a).

The maximal fidelity $F_{\rm EWSS}(\tau_{\rm EWSS})$ to the EWSS monotonically decreases with respect to J, which can be well fitted for $J \geqslant 400$ to

$$F_{\rm EWSS}(\tau_{\rm EWSS}) = \left(\frac{0.0298 \pm 0.0001}{J^{0.621\pm0.001}} + 0.995\right)^2. \tag{6}$$

Here, the numerical results throughout the article contain errors less than the order of the last digit, unless otherwise stated. In the large-J limit, $F_{\rm EWSS}(\tau_{\rm EWSS})$ in Eq. (6) converges to $\sim$0.990, which is interesting because the EWSS is not easy

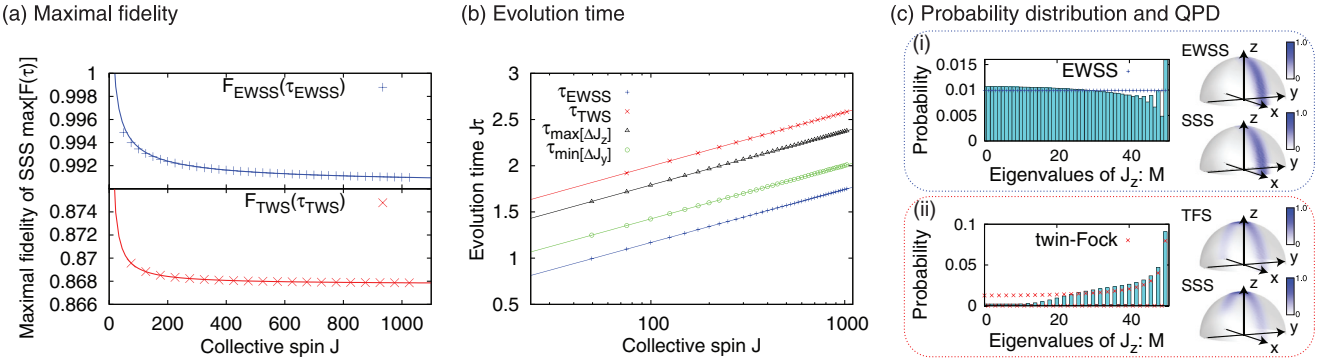

FIG. 2. (Color online) (a) Maximal fidelity of the SSS to the EWSS and that to the twin-Fock state as functions of the collective spin J. The blue solid curve is given by Eq. (6) and well fitted to the region of $J \geqslant 400$, while the red solid curve is given by Eq. (8) and shows excellent agreement with the plot points. (b) Squeezing-evolution time $\tau_{\rm EWSS}$, $\tau_{\rm TFS}$, $\tau_{\max[\Delta J_z]}$, and $\tau_{\min[\Delta J_y]}$. Here, $\tau_{\max[\Delta J_z]}$ maximizes the quantum fluctuations in J_z and $\tau_{\min[\Delta J_y]}$ minimizes the quantum fluctuations in J_y, respectively. The results of $\tau_{\rm EWSS}$, $\tau_{\rm TFS}$, and $\tau_{\max[\Delta J_z]}$ are well fitted to Eqs. (7), (9), and (18), which are plotted by the solid curves for all J's. (c) (i) Probability distributions and QPD functions for the EWSS and the SSS optimized to the EWSS for $J = 50$. The QPD functions are plotted on the upper hemispheres of the Bloch spheres and their magnitudes are expressed by the thickness of the blue color. Note that these QPDs are symmetric about the equator. The probability distribution for the SSS with respect to the eigenvalues of $\hat{J}_z$ is expressed by blue boxes. Here the blue dots of the probability distribution for the EWSS are plotted at $(2J+1)^{-1}$. (ii) Probability distributions and QPD functions of the twin-Fock state and the SSS optimized to the twin-Fock state for $J = 50$. The probability distribution for the SSS with respect to the eigenvalues of $\hat{J}_z$ is expressed by blue boxes with red crosses of the probability distribution shown for the twin-Fock state.

to implement experimentally. We also plot the evolution time τ_{EWSS} that optimizes the fidelity F_{EWSS} in Fig. 2(b), which can be well fitted to a function of J as

$$\tau_{\mathrm{EWSS}} = \frac{\ln(1.10J)}{4.02J}, \tag{7}$$

for all J. Here, the fidelity $F_{\mathrm{EWSS}}(\tau)$ for $\tau \sim \tau_{\mathrm{EWSS}}$ can be well fitted to the Lorentzian function with a FWHM of $\sim 2/(3J)$, as shown in Fig. 1. Hence, a small change in τ reduces $F_{\mathrm{ESSS}}(\tau)$, which may lead to practical difficulties; however, we can expect to achieve high fidelity by setting χ sufficiently small.

Meanwhile, $F_{\mathrm{TFS}}(\tau_{\mathrm{TFS}})$ monotonically decreases with respect to J similarly to the EWSS case, as shown in the lower panel of Fig. 2(a), which can be well fitted to

$$F_{\mathrm{TFS}}(\tau_{\mathrm{TFS}}) = \left(\frac{0.0743}{J^{1.00}} + 0.932\right)^2. \tag{8}$$

Equation (8) converges to ~ 0.868 in the large J limit. The evolution time τ_{TFS} is plotted with respect to J in Fig. 2(b), which can be well fitted to

$$\tau_{\mathrm{TFS}} = \frac{\ln[(25.2 \pm 0.2)J]}{3.93J}. \tag{9}$$

As shown in Fig. 1, the fidelity $F_{\mathrm{TFS}}(\tau)$ has a peak around $\tau \sim \tau_{\mathrm{TFS}}$ which is broader than the Gaussian or Lorentzian functions. This implies that we can expect to achieve high fidelity in a manner similar to the case of τ_{EWSS}.

To discuss the deviations of $F_{\mathrm{EWSS}}(\tau_{\mathrm{EWSS}})$ and $F_{\mathrm{TFS}}(\tau_{\mathrm{TFS}})$ from $F = 1$, we plot the quasiprobability distribution (QPD) and the probability distributions for the SSSs optimized to the EWSS and the twin-Fock state for $J = 50$ in Fig. 2(c)(i). Here, the QPD function [5] and the probability distribution of the state $|\Psi_X\rangle$ are respectively defined as $\tilde{P}_X(\varphi,\theta) = |\langle\Psi_{\mathrm{CSS}}(\varphi,\theta)|\Psi_X\rangle|^2$ and $P_X(M) = |\langle J,M|\Psi_X\rangle|^2$, where φ and θ in the QPD are the azimuth and polar angles of the sphere with a unit radius. The probability distribution of $|\Psi_{\mathrm{SSS}}(\tau_{\mathrm{EWSS}})\rangle_x$ in Fig. 2(c)(i) oscillates around $|M| \sim J$, unlike that of the EWSS in Fig. 2(c)(i), which may decrease $F_{\mathrm{EWSS}}(\tau_{\mathrm{EWSS}})$. On the other hand, both the QPD and the probability distribution of $|\Psi_{\mathrm{SSS}}(\tau_{\mathrm{TFS}})\rangle_x$ are distinct from those of the twin-Fock state, as shown in Fig. 2(c)(ii): The QPD of $|\Psi_{\mathrm{SSS}}(\tau_{\mathrm{TFS}})\rangle_x$ shows a gap at $(\varphi,\theta) \sim (\pi,\pi/2)$ and the probability distribution in Fig. 2(c)(ii) has a dip structure around $M = 0$, which contributes to the degradation of the fidelity for large J.

Here, we discuss the effect of the linear Zeeman effect on the fidelity. The fidelity does not change so much if the magnetic field $\boldsymbol{B}$ is oriented in the z axis and satisfies

$$\frac{2\gamma_B B \ln J}{J} \ll 1 \tag{10}$$

for $\tau \sim \ln J/J$ in Eqs. (7) and (8), which is shown in the Appendix.

IV. PRECISIONS OF MEASUREMENTS USING SQUEEZED SPIN STATES

Then, we evaluate the SSS for high-precision measurements using the Cramér-Rao inequality. The Cramér-Rao inequality gives the lower bound of the standard deviation of unbiased measurements [36–39]. Let us assume that we perform a positive operator-valued measure (POVM) on a value X, repeating it N_{msr} times to estimate X from N_{msr} outcomes. The statistical deviation of X's unbiased estimator X_{est} is defined as $\delta X \equiv X_{\mathrm{est}}/|d\langle\langle X_{\mathrm{est}}\rangle\rangle_X/dX| - X$, where $\langle\langle\rangle\rangle_X$ represents the expectation value over the N_{msr}-times measurements. Since we assume an unbiased measurement, the precision of the measurement, i.e., the standard deviation of X_{est}, can be expressed in terms of δX as $\sigma_X \equiv (N_{\mathrm{msr}}\langle\langle(\delta X)^2\rangle\rangle_X)^{1/2}$. The standard deviation σ_X for any unbiased measurement satisfies the Cramér-Rao inequality, that is,

$$\sigma_X \geqslant \mathcal{I}_X{}^{-1/2}, \tag{11}$$

the lower bound of which gives the optimal precision. Here $\mathcal{I}_X$ is the quantum Fisher information [38,39], which has an upper bound determined by the input state interacting with X. Since we are interested in the fundamental properties of high-precision measurements, we assume the input state to be pure, $\hat{\rho}_{\mathrm{inp}} = |\Psi_{\mathrm{inp}}\rangle\langle\Psi_{\mathrm{inp}}|$ [33,34,39]. In this case, the quantum Fisher information satisfies

$$\mathcal{I}_X \leqslant 4\langle\hat{\rho}'^2_{\mathrm{inp}}\rangle_{\mathrm{inp}}, \tag{12}$$

where the operator $\hat{\rho}'_{\mathrm{inp}}$ is the X derivative of $\hat{\rho}_{\mathrm{inp}}$ and the expectation value $\langle\hat{O}\rangle_{\mathrm{inp}} \equiv \mathrm{Tr}[\hat{\rho}_{\mathrm{inp}}\hat{O}]$. Combining inequalities (11) and (12), we obtain the inequality satisfied by the standard deviation:

$$\sigma_X \geqslant \frac{1}{2\langle\hat{\rho}'^2_{\mathrm{inp}}\rangle^{1/2}_{\mathrm{inp}}}. \tag{13}$$

We use inequality (13) to obtain the optimal sensitivity for the estimation of the magnetic field $\boldsymbol{B}$ along the z axis [34,35]. The system evolves under the Hamiltonian $\hat{H}_{\boldsymbol{B}} = -\hbar\gamma_s B\hat{J}_z$, where γ_s denotes the gyromagnetic ratio and B is the magnitude of $\boldsymbol{B}$. To estimate B, a state $\hat{\rho}_{\mathrm{inp}}(0)$ is prepared at the initial time, and the state after a certain time t under $\hat{H}_{\boldsymbol{B}}$, $\hat{\rho}_{\mathrm{inp}}(t)$, is used as the input state of the parameter estimation. Since the upper bound of the Fisher information is given by Eq. (12), we obtain $\mathcal{I}_B(t) \leqslant 4(\gamma_s t)^2\langle(\Delta J_z)^2\rangle_{\mathrm{inp}}$ by substituting $\hat{\rho}_{\mathrm{inp}}(t)$ into the inequality (12). Here the quantum fluctuations in an observable $\hat{O}$ is defined as $\langle(\Delta O)^2\rangle \equiv \langle\hat{O}^2\rangle - \langle\hat{O}\rangle^2$. The Cramér-Rao inequality in Eq. (13) is now given by

$$\sigma_B \geqslant \frac{1}{2\gamma_s t\langle(\Delta J_z)^2\rangle^{1/2}_{\mathrm{inp}}}, \tag{14}$$

implying that the measurement precision is determined by $\langle(\Delta J_z)^2\rangle^{1/2}_{\mathrm{inp}}$ and the Heisenberg-limited sensitivity can be achieved when $\langle(\Delta J_z)^2\rangle^{1/2}_{\mathrm{inp}}$ is linear to J; hence we analyze the scaling law of $\langle(\Delta J_z)^2\rangle^{1/2}_{\mathrm{inp}}$ instead of inequalities (14) to discuss the sensitivity.

The quantum fluctuations in $\hat{J}_z$ are numerically calculated for the SSSs optimized to the EWSS and the twin-Fock state, and the SSS maximizing $\langle(\Delta J_z)^2\rangle^{1/2}_{\mathrm{inp}}$ with respect to τ, and they are plotted in Fig. 3. For the SSS optimized to the EWSS, $\langle(\Delta J_z)^2\rangle^{1/2}_{\mathrm{SSS}}(\tau_{\mathrm{EWSS}})$ is well fitted for $J \geqslant 300$ to

$$\langle(\Delta J_z)^2\rangle^{1/2}_{\mathrm{SSS}}(\tau_{\mathrm{EWSS}}) = 0.557(J + 1.03)^{1.00}, \tag{15}$$

which can achieve the Heisenberg-limited sensitivity in Eq. (14). The linear coefficient in Eq. (15) is close to that

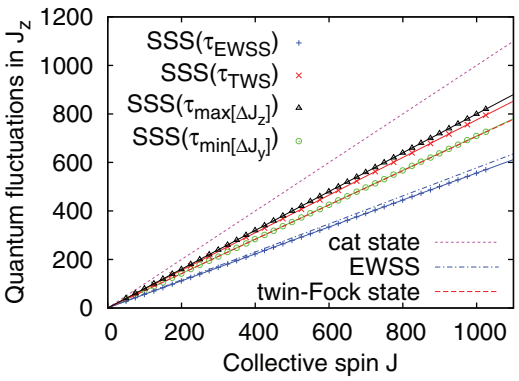

FIG. 3. (Color online) Quantum fluctuations in $\hat{J}_z$ for the SSSs as functions of the collective spin J. Quantum fluctuations $\langle(\Delta\hat{J}_z)^2\rangle_{\rm SSS}^{1/2}$ for the SSSs optimized to the EWSS and the twin-Fock state, the maximal quantum fluctuations in $\hat{J}_z$, and the minimal quantum fluctuations in $\hat{J}_y$ which are compared to those for the cat state, the EWSS, and the twin-Fock state. Quantum fluctuations $\langle(\Delta\hat{J}_z)^2\rangle_{\rm SSS}^{1/2}(\tau_{\rm EWSS})$ are well fitted to Eq. (15) for $J \geqslant 400$, and $\langle(\Delta\hat{J}_z)^2\rangle_{\rm SSS}^{1/2}(\tau_{\rm TFS})$ and the maximal $\langle(\Delta\hat{J}_z)^2\rangle_{\rm SSS}^{1/2}$ are well fitted for all J to Eqs. (16) and (17), respectively.

for the EWSS as shown in Fig. 3, since $\langle(\Delta J_z)^2\rangle_{\rm EWSS}^{1/2} = \sqrt{J(J+1)/3} \simeq 0.577J$ in the large-J limit. The difference in the linear coefficients for the EWSS and $|\Psi_{\rm SSS}(\tau_{\rm EWSS})\rangle$ in Eq. (15) is as small as 3.59%, which indicates that spin squeezing through two-axis countertwisting can be used to generate an approximate state of the EWSS for high-precision measurements. Similarly, $\langle(\Delta J_z)^2\rangle_{\rm SSS}^{1/2}(\tau_{\rm TFS})$ is well fitted to the function that shows the Heisenberg-limit scaling of the sensitivity,

$$\langle(\Delta J_z)^2\rangle_{\rm SSS}^{1/2}(\tau_{\rm TFS}) = 0.775(J+0.494)^{1.00}, \qquad (16)$$

which is smaller than that for the twin-Fock state by a factor of 0.912, since $\langle(\Delta J_z)^2\rangle_{\rm TFS}^{1/2} \simeq \sqrt{J(J+1)/2} \simeq 0.707J$ in the large-J limit [9,35], as shown in Fig. 3. The quantum fluctuations $\langle(\Delta J_z)^2\rangle_{\rm SSS}^{1/2}$ maximized with respect to τ is also well fitted to the Heisenberg-limit scaling of the sensitivity, that is,

$$\langle(\Delta J_z)^2\rangle_{\rm SSS}^{1/2}(\tau_{\max[\Delta J_z]}) = 0.799(J+0.453)^{1.00}, \qquad (17)$$

with the corresponding evolution time of $\tau_{\max[\Delta J_z]}$, which can be well fitted to

$$\tau_{\max[\Delta J_z]} = \frac{\ln(11.5J)}{3.94J} \qquad (18)$$

for all J. As shown in Fig. 1, the local maximum of the quantum fluctuations $\langle(\Delta J_z)^2\rangle_{\rm SSS}^{1/2}$ is broader than the Gaussian and Lorentzian functions; hence we can expect that a good optimal Fisher information can be achieved by a manner similar to the case of $\tau_{\rm EWSS}$ and $\tau_{\rm TFS}$ in Eqs. (7) and (9).

The maximal Fisher information in Eq. (17) is larger than the optimal Fisher information at $\tau = \tau_{\min[\Delta J_y]}$ when the quantum fluctuations in $\hat{J}_y$ are minimized, as shown in Fig. 3. The Cramér-Rao inequality in Eq. (14) gives the best precision when the state is the cat state [or the Greenberger-Horne-Zeilinger (GHZ) state], namely, the superposition state of the highest and lowest weight states, i.e., $|\Psi_{\rm CAT}\rangle = (|J,J\rangle + |J,-J\rangle)/\sqrt{2}$. and the quantum fluctuations in $\hat{J}_z$ are given by $\langle(\Delta J_z)^2\rangle_{\rm CAT}^{1/2} = J$ [35]. It is clear that the sensitivity using the SSSs cannot reach the best sensitivity that the optimal superposition state gives for the same J. However, the sensitivity by the SSSs can achieve higher sensitivities than the ones achievable by the EWSS, the twin-Fock state, or the minimal quantum fluctuation state, all of which are candidate state measurements.

V. SUMMARY

To summarize, we have numerically analyzed the time evolution of SSSs under the two-axis countertwisting interaction and the sensitivity in magnetic-field measurements. We find that at time $\tau_{\rm EWSS}$ the SSS can be approximately represented as the EWSS because of its high fidelity of 0.990 in the large-J limit, and after that, at the time $\tau_{\rm TFS}$ the SSS becomes close to the twin-Fock state with a fidelity of 0.868 in the large-J limit. We have also calculated the sensitivity defined by the lower bound of the Cramér-Rao inequality and have shown that the SSS reaches the Heisenberg limit and exceeds the sensitivity limit given with the EWSS and the twin-Fock state, though it does not reach the sensitivity limit of the optimal state $|\Psi_{\rm CAT}\rangle$. To evaluate the feasibility, we still have to consider noise effects involved in the squeezing; however, as there are theoretical proposals to realize a two-axis countertwisting interaction in Bose-Einstein condensates and one-axis twisting has already been demonstrated beyond the standard quantum limit, we can expect that it will be more realistic to use SSSs than other states to realize the Heisenberg limit. The time required to achieve the best sensitivity for the SSS is $\tau_{\max[\Delta J_z]} = \ln(11.5J)/(3.94J)$; thus, by adjusting the time and the size of the collective spin, we may minimize the effect of noise, though further research is necessary to clarify the noise effects (e.g., Refs. [10,27,28,40,41]).

ACKNOWLEDGMENTS

The authors thank Dr. M. Negoro. This work is supported by National Institute of Information and Communications Technology Project No. 158A, Grant-in-Aid for Scientific Research S Grant No. 25220601 from Japan Society for Promotion of Science (JSPS), Nippon Telegraph and Telephone Corporation, and Grant-in-Aid for Scientific Research B Grant No. 26287088 from JSPS.

APPENDIX: DERIVATION OF EQ. (10)

When a static magnetic field $\boldsymbol{B}$ is applied, the Hamiltonian becomes $\hat{H}_{\rm TAT} + \hat{H}_{\boldsymbol{B}}$, where

$$\hat{H}_{\boldsymbol{B}} = -\hbar\gamma_B B\left(\frac{e^{i\varphi}}{2}\sin\theta\,\hat{J}_+ + \frac{e^{-i\varphi}}{2}\sin\theta\,\hat{J}_- + \cos\theta\,\hat{J}_z\right), \qquad (A1)$$

and the Schrödinger equation in the rotating frame of $\hat{H}_{-\boldsymbol{B}}$ can be expressed as

$$\frac{d|\Psi_{\rm SSS}(\tau)\rangle_{\rm rot}}{d\tau} = \frac{1}{i\hbar}\hat{U}_{-\boldsymbol{B}}(\tau)\hat{H}_{\rm TAT}\hat{U}_{-\boldsymbol{B}}^{\dagger}(\tau)|\Psi_{\rm SSS}(\tau)\rangle_{\rm rot}, \qquad (A2)$$

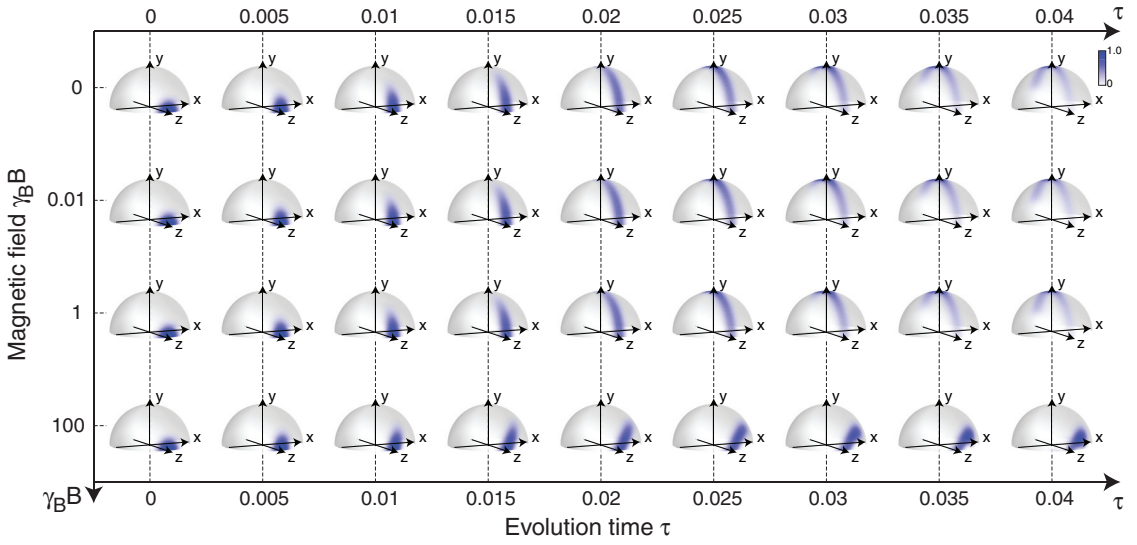

FIG. 4. (Color online) Quasiprobability distributions of $|\Psi_{\rm SSS}(\tau)\rangle$ for $J = 50$ and $\chi = 1$ plotted against the evolution time τ and the magnetic field B along the z axis. Unlike the cases of $\gamma_B B = 0.01$ and 1, the quasiprobability distributions for $B = 100$ cannot be obtained by a Euler rotation of the quasiprobability distribution for $B = 0$, and $|\Psi_{\rm SSS}(\tau)\rangle$ for $\gamma_B B = 100$ does not have high fidelity to the EWSS or the twin-Fock state. The quasiprobability distribution of the squeezed spin state for $\gamma_B B = 100$ and $\tau = 0.04$ distributes around the fixed points of the mean-field dynamics under $\hat{H}_{\rm TAT} + \hat{H}_{\boldsymbol{B}}$.

where $\hat{U}_{-\boldsymbol{B}}(\tau) \equiv \exp[\hat{H}_{-\boldsymbol{B}}\tau/i\hbar]$ and $|\Psi_{\rm SSS}\rangle_{\rm rot} \equiv \hat{U}_{-\boldsymbol{B}}(\tau)|\Psi_{\rm SSS}\rangle$. If the magnetic field $\boldsymbol{B}$ is applied along the z axis, the two-axis countertwisting interactions in the rotating frame depend on τ as follows:

$$\hat{U}_{-\boldsymbol{B}}(\tau)\hat{H}_{\rm TAT}\hat{U}^{\dagger}_{-\boldsymbol{B}}(\tau) = \frac{\hbar\chi}{2i}(e^{-2i\gamma_B B\tau}\hat{J}_+^2 - e^{2i\gamma_B B\tau}\hat{J}_-^2), \tag{A3}$$

which implies that the fidelity does not change drastically if $2\gamma_B B\tau \ll 1$ in Eq. (10). By numerically solving Eq. (A2), we obtain $|\Psi_{\rm SSS}(\tau)\rangle$ for $J = 50$, $\chi = 1$, and the magnetic field of $\gamma_B B = 0$, 0.01, 1, and 100. In cases of $\gamma_B B = 0.01$ and 1, the condition $2\gamma_B B\tau \ll 1$ is satisfied and the fidelity does not decrease significantly. On the other hand, $2\gamma_B B\tau \sim 1$ for the case of $\gamma_B B = 100$ and the fidelity drastically decreases, as can be seen from the quasiprobability distributions for $\gamma_B B = 100$ in Fig. 4.

[1] H. Aasi *et al.*, Nat. Photonics **7**, 613 (2013).
[2] M. A. Taylor, J. Janousek, V. Daria, J. Knittel, B. Hage, H.-A. Bachor, and W. P. Bowen, Phys. Rev. X **4**, 011017 (2014).
[3] T. Tilma, S. Hamaji, W. J. Munro, and K. Nemoto, Phys. Rev. A **81**, 022108 (2010).
[4] B. Yurke and D. Stoler, Phys. Rev. Lett. **57**, 13 (1986).
[5] M. Kitagawa and M. Ueda, Phys. Rev. A **47**, 5138 (1993).
[6] M. J. Holland and K. Burnett, Phys. Rev. Lett. **71**, 1355 (1993).
[7] J. J. Bollinger, W. M. Itano, D. J. Wineland, and D. J. Heinzen, Phys. Rev. A **54**, R4649 (1996).
[8] A. Sørensen, L.-M. Duan, J. I. Cirac, and P. Zoller, Nature (London) **409**, 63 (2001).
[9] A. André, L.-M. Duan, and M. D. Lukin, Phys. Rev. Lett. **88**, 243602 (2002).
[10] J. K. Stockton, J. M. Geremia, A. C. Doherty, and H. Mabuchi, Phys. Rev. A **67**, 022112 (2003).
[11] D. Leibfried, M. D. Barrett, T. Schaetz, J. Britton, J. Chiaverini, W. M. Itano, J. D. Jost, C. Langer, and D. J. Wineland, Science **304**, 1476 (2004).
[12] V. Giovannetti, S. Lloyd, and L. Maccone, Science **306**, 1330 (2004).
[13] B. Lücke, M. Scherer, J. Kruse, L. Pezzé, F. Deuretzbacher, P. Hyllus, O. Topic, J. Peise, W. Ertmer, J. Arlt, L. Santos, A. Smerzi, and C. Klempt, Science **334**, 773 (2011).
[14] R. J. Sewell, M. Napolitano, N. Behbood, G. Colangelo, F. M. Ciurana, and M. W. Mitchell, Phys. Rev. X **4**, 021045 (2014).
[15] J. Hald, J. L. Sørensen, C. Schori, and E. S. Polzik, Phys. Rev. Lett. **83**, 1319 (1999).
[16] A. Kuzmich, L. Mandel, J. Janis, Y. E. Young, R. Ejnisman, and N. P. Bigelow, Phys. Rev. A **60**, 2346 (1999); A. Kuzmich, L. Mandel, and N. P. Bigelow, Phys. Rev. Lett. **85**, 1594 (2000).
[17] J. M. Geremia, J. K. Stockton, A. C. Doherty, and H. Mabuchi, Phys. Rev. Lett. **91**, 250801 (2003).
[18] J. Estève, C. Gross, A. Weller, S. Giovanazzi, and M. K. Oberthaler, Nature (London) **455**, 1216 (2008).
[19] I. D. Leroux, M. H. Schleier-Smith, and V. Vuletić, Phys. Rev. Lett. **104**, 073602 (2010); M. H. Schleier-Smith, I. D. Leroux, and V. Vuletić, Phys. Rev. A **81**, 021804(R) (2010).
[20] C. Gross, T. Zibold, E. Nicklas, J. Estève, and M. K. Oberthaler, Nature (London) **464**, 1165 (2010).
[21] M. F. Riedel, P. Böhi, Y. Li, T. W. Hänsch, A. Sinatra, and P. Treutlein, Nature (London) **464**, 1170 (2010).
[22] Z. Chen, J. G. Bohnet, S. R. Sankar, J. Dai, and J. K. Thompson, Phys. Rev. Lett. **106**, 133601 (2011).
[23] C. D. Hamley, C. S. Gerving, T. M. Hoang, E. M. Bookjans, and M. S. Chapman, Nat. Phys. **8**, 305 (2012).
[24] R. Inoue, S.-I.-R. Tanaka, R. Namiki, T. Sagawa, and Y. Takahashi, Phys. Rev. Lett. **110**, 163602 (2013).

[25] S. D. Bennett, N. Y. Yao, J. Otterbach, P. Zoller, P. Rabl, and M. D. Lukin, Phys. Rev. Lett. **110**, 156402 (2013).
[26] K. Helmerson and L. You, Phys. Rev. Lett. **87**, 170402 (2001).
[27] A. André and M. D. Lukin, Phys. Rev. A **65**, 053819 (2002).
[28] L. K. Thomsen, S. Mancini, and H. M. Wiseman, J. Phys. B **35**, 4937 (2002).
[29] H. T. Ng, C. K. Law, and P. T. Leung, Phys. Rev. A **68**, 013604 (2003).
[30] M. Zhang, K. Helmerson, and L. You, Phys. Rev. A **68**, 043622 (2003).
[31] P. Cappellaro and M. D. Lukin, Phys. Rev. A **80**, 032311 (2009).
[32] Y. C. Liu, Z. F. Xu, G. R. Jin, and L. You, Phys. Rev. Lett. **107**, 013601 (2011).
[33] L. Pezzé and A. Smerzi, Phys. Rev. Lett. **102**, 100401 (2009).
[34] B. A. Chase, B. Q. Baragiola, H. L. Partner, B. D. Black, and J. M. Geremia, Phys. Rev. A **79**, 062107 (2009).
[35] J. Maa, X. Wanga, C. P. Suna, and F. Nori, Phys. Rep. **509**, 89 (2011).
[36] C. R. Rao, Bull. Calcutta Math. Soc. **37**, 81 (1945).
[37] H. Cramér, *Mathematical Methods of Statistics* (Princeton University Press, Princeton, NJ, 1946), Chap. 33.
[38] S. L. Braunstein and C. M. Caves, Phys. Rev. Lett. **72**, 3439 (1994).
[39] S. L. Braunstein, C. M. Caves, and G. J. Milburn, Ann. Phys. **247**, 135 (1996).
[40] T. E. Lee, S. Gopalakrishnan, and M. D. Lukin, Phys. Rev. Lett. **110**, 257204 (2013).
[41] T. E. Lee, C.-K. Chan, and S. F. Yelin, Phys. Rev. A **90**, 052109 (2014).